Propagation of Strong Rainfall Events from Southeastern South America to the Central Andes

Niklas Boers,[*,+] Henrique M. J. Barbosa,[#] Bodo Bookhagen,[@] José A. Marengo,[&] Norbert Marwan,[*] and Jürgen Kurths[*,+,**]

[*] *Potsdam Institute for Climate Impact Research, Potsdam, Brandenburg, Germany*
[+] *Department of Physics, Humboldt University Berlin, Berlin, Germany*
[#] *Institute of Physics, University of São Paulo, São Paulo, Brazil*
[@] *Institute of Earth and Environmental Science, University of Potsdam, Potsdam, Germany*
[&] *Center for Monitoring and Early Warning of Natural Disasters (CEMADEN), Cachoeira Paulista, São Paulo, Brazil*
[**] *Department of Control Theory, Nizhny Novgorod State University, Nizhny Novgorod, Russia*

ABSTRACT

Based on high-spatiotemporal-resolution data, the authors perform a climatological study of strong rainfall events propagating from southeastern South America to the eastern slopes of the central Andes during the monsoon season. These events account for up to 70% of total seasonal rainfall in these areas. They are of societal relevance because of associated natural hazards in the form of floods and landslides, and they form an intriguing climatic phenomenon, because they propagate against the direction of the low-level moisture flow from the tropics. The responsible synoptic mechanism is analyzed using suitable composites of the relevant atmospheric variables with high temporal resolution. The results suggest that the low-level inflow from the tropics, while important for maintaining sufficient moisture in the area of rainfall, does not initiate the formation of rainfall clusters. Instead, alternating low and high pressure anomalies in midlatitudes, which are associated with an eastward-moving Rossby wave train, in combination with the northwestern Argentinean low, create favorable pressure and wind conditions for frontogenesis and subsequent precipitation events propagating from southeastern South America toward the Bolivian Andes.

1. Introduction

Southeastern South America (SESA) is frequently affected by severe thunderstorms in the form of mesoscale convective systems (MCS), which add substantial contributions to the total rainfall sums in this region (Durkee et al. 2009; Durkee and Mote 2009). Some particular cases of these MCS have been observed to form in series, with overall convective development initiating in SESA and subsequently propagating northwestward (Anabor et al. 2008). The general influence of cold fronts on large-scale circulation and associated precipitation anomalies has been

thoroughly studied (e.g., Kousky 1979; Kiladis and Weickmann 1992; Liebmann et al. 1999; Siqueira and Machado 2004; Siqueira et al. 2005). In particular, northward migrating convective disturbances over SESA have been associated with southerly incursions of cold air from midlatitudes (Garreaud and Wallace 1998; Garreaud 2000). These authors showed that the convective bands add an important contribution to overall rainfall amounts and occur with a frequency of roughly 7–12 days. Related precipitation events at the eastern central Andes (ECA) have been addressed in (Montes de Oca 1995). However, these studies are based on data with coarse temporal and spatial resolution (daily, $2.5° \times 2.5°$), which might not be good enough to adequately resolve the responsible physical mechanism including possible feedback contributions (Garreaud and Wallace 1998). Using high-spatiotemporal-resolution data, we intend to further deepen the understanding of

these propagation events with special focus on the temporal order of the atmospheric features leading to their occurrence.

In a recent study (Boers et al. 2014a), techniques from complex network theory were developed and applied to identify dominant synchronization patterns of extreme rainfall (above the 99th percentile of 3-h time steps). The authors found that during the monsoon season in South America [December–February (DJF)], extreme rainfall in SESA propagates northwestward toward the slopes of the ECA under certain atmospheric conditions. They showed that these propagation events were associated with frontal systems originating from the south and causing the initial precipitation in SESA. Furthermore, it was shown how this information can be used for a statistical forecast of more than 60% of extreme rainfall events and associated floods and landslides at the ECA.

To better understand the temporal order and relations between the occurrence of strong rainfall, pressure anomalies, and variability of the low-level flow, here we will analyze the atmospheric conditions favoring the propagation of strong precipitation along the typical propagation path from SESA to ECA using 3-hourly rainfall data. This path is delineated by the spatial boxes 1–7 in Fig. 1. First, we show that this propagation pattern is a rather typical feature of the South American monsoon system (SAMS). Then we analyze 3-hourly composites of rainfall data obtained from the Tropical Rainfall Measuring Mission satellite product in its newest version (TRMM 3B42 V7; Huffman et al. 2007), as well as 3-hourly geopotential height and wind fields at 850 hPa obtained from NASA's Modern-Era Retrospective Analysis for Research and Applications (MERRA) dataset (Rienecker et al. 2011). These composites will be constructed for the following temporal subsets, where we call rainfall *strong* if the spatial average over the respective spatial boxes is above the 90th percentile of all DJF time steps with rainfall rates larger than $0 \, mm \, h^{-1}$: 1) times of strong rainfall in SESA that subsequently propagates to the ECA; 2) times of strong rainfall in SESA not propagating to the ECA; 3) times for which strong rainfall at the ECA is preceded by strong rainfall at SESA; and 4) times for which strong rainfall at the ECA is not preceded by strong rainfall in SESA. We will show that our results are, in principle, consistent with the results of Garreaud and Wallace (1998), Garreaud (2000), and Siqueira et al. (2005). However, several additional details concerning the interplay of frontal systems, orography, and climatological low pressure cells in the area can be deduced from our study because of higher-spatiotemporal-resolution data and different composite selections at process-relevant times.
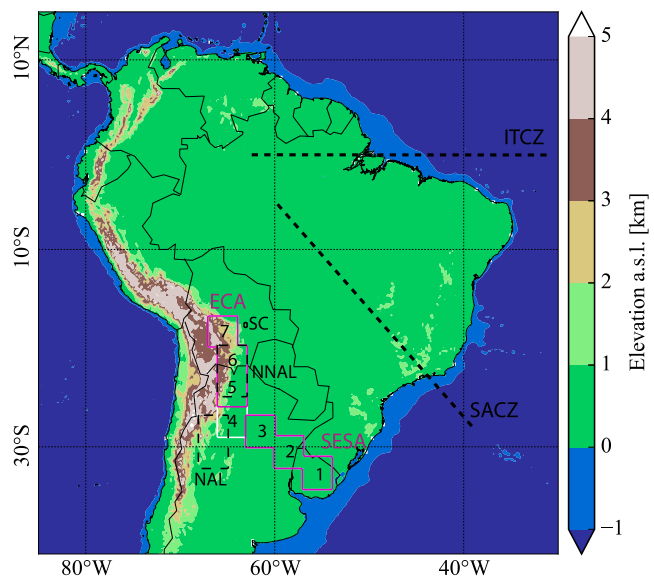

FIG. 1. Topography and key features of the SAMS, including the ITCZ and the SACZ. The typical propagation pathway of surface rainfall is indicated by the boxes 1–7. The region SESA (boxes 1–3) and the ECA (boxes 5–7) are delineated by magenta boxes. The study regions at Santa Cruz de la Sierra (SC), at NAL, and NNAL are delineated by black dashed lines.

2. Climatic setting

The core monsoon season in South America from December through February (Marengo et al. 2012) is characterized by a southward displacement of the intertropical convergence zone (ITCZ; see Fig. 1). Trade winds, further strengthened by the differential heating between ocean and land (Zhou and Lau 1998), are responsible for enhanced moisture flow from the tropical Atlantic Ocean to the continent (Rodwell and Hoskins 2001; Liebmann and Mechoso 2011). After crossing the Amazon basin and recharging its moisture content from evapotranspiration (Eltahir and Bras 1994), this low-level flow is blocked by the Andes mountain range to the west, resulting in a southward turn of the wind directions (Byerle and Paegle 2002). The direction of the subsequent low-level flow toward the subtropics depends on thermodynamic (Berbery and Collini 2000) as well as synoptic conditions in subtropical South America and can range from SESA (Nicolini et al. 2002; Salio et al. 2007) to the South Atlantic convergence zone (SACZ; Carvalho et al. 2004, 2011). Strong southward anomalies of the flow are associated with the establishment of the South American low-level jet (SALLJ; Marengo et al. 2004), which is partly controlled by the Chaco low over Bolivia and the northwestern Argentinean low (NAL) (Seluchi and Saulo 2003; Ferreira et al. 2003; Saulo et al. 2004). Southward anomalies of the low-level flow have been found to be responsible for enhanced rainfall at the ECA: strengthened winds from the Amazon toward the Andes carry moist air

masses to higher elevations and rainfall occurs at the Andean slopes as a consequence of orographic lifting (Bookhagen and Strecker 2008; Giovannettone and Barros 2009; Romatschke and Houze 2013).

A pronounced southward component of the flow east of the Andes (as during SALLJ events) is also related to enhanced rainfall in SESA (Nicolini et al. 2002; Díaz and Aceituno 2003) while, on the other hand, a stronger eastward component goes alongside with enhanced rainfall in the SACZ (Liebmann et al. 2004). The oscillation in rainfall amounts between the SESA and the SACZ area is usually referred to as the South American rainfall dipole (Nogués-Paegle and Mo 1997; Boers et al. 2014b). The variability in subtropical moisture flow is associated with cold fronts approaching from the south (Siqueira et al. 2005), caused by eastward propagating Rossby waves originating from the western Pacific Ocean (Lenters and Cook 1999; Renwick and Revell 1999; Carvalho et al. 2004). A large fraction of rainfall in SESA is contributed by MCS (Durkee et al. 2009; Durkee and Mote 2009). The occurrence of these MCS in the La Plata basin has been associated with southward anomalies of the low-level flow from the tropics (Salio et al. 2007), but the causal relationship between anomalies of the low-level flow from the Amazon to SESA and MCS development in SESA has not been determined.

3. Data

For all climatic variables, we focused on the area from 40° to 5°S and from 85° to 30°W and the DJF seasons in the time period from 1998 to 2012. For rainfall data, we employ the 3-hourly TRMM 3B42 V7 (Huffman et al. 2007) with a spatial resolution of 0.25° × 0.25°. For pressure and wind data, we use 3-hourly instantaneous fields from MERRA (Rienecker et al. 2011) with a spatial resolution of 1.25° × 1.25°.

4. Methods

In Boers et al. (2014a), a sequence of seven geographic boxes was identified along which extreme rainfall events (above the 99th percentile) propagate from SESA to ECA (Fig. 1). In contrast to the nomenclature used in the previous publication, we will refer to the first three boxes of this sequence as SESA and to the last three boxes as ECA in this manuscript.

We compute the spatial average of rainfall in each of the seven boxes for each 3-hourly time step. Time steps during DJF for which the sum of rainfall in the three boxes constituting SESA (ECA) is above the 90th percentile of wet times (rainfall > 0 mm h^{-1}) we will call SESA times (ECA times). In the remainder of this study, we will call rainfall rates strong if these conditions are fulfilled.

As mentioned above, we are interested in the following 4 different regimes:

1) SESA-ECA times: times at which there is strong rainfall in SESA followed (within the next 6–36 h) by strong rainfall in ECA,
2) SESA-NO-ECA times: times at which there is strong rainfall in SESA not followed by strong rainfall in ECA,
3) ECA-SESA times: times at which there is strong rainfall in ECA preceded (within the previous 6–36 h) by strong rainfall in SESA, and
4) ECA-NO-SESA times: times at which there is strong rainfall in ECA not preceded by strong rainfall in SESA.

We will construct composites of rainfall and geopotential height and wind fields separately for all four regimes in order to explain the northwestward propagation of rainfall from SESA to ECA. Note that SESA-ECA times and ECA-SESA times are defined in a similar manner, but the first are centered at the times of peak rainfall in SESA, while the latter are centered at the times of peak rainfall in ECA. Since the delays between these two temporal subsets are not constant, ECA-SESA times are not simply shifted SESA-ECA times.

Events of an active low-level jet were identified on a 3-hourly basis following Marengo et al. (2004), who suggested the following conditions based on the Bonner criterion 1 (Bonner 1968): 1) wind speeds at 850 hPa equal or larger than 12 m s^{-1} with southward meridional component larger than the zonal component and 2) wind speeds at 700 hPa at least 6 m s^{-1} slower than at 850 hPa. Here, also following Salio et al. (2007), we applied these conditions to Santa Cruz at 17°S, 62°W for the SALLJ. To investigate possible influence of the actual wind speeds, we separately identified events for which wind speeds at 850 hPa are equal to or larger than 9, 12, 15, and 18 m s^{-1}.

5. Results

a. Composite fields for the four regimes

For each DJF season, there are 736 time steps of 3 h. Out of these, there are, on average, 56 SESA-ECA times, 5 SESA-NO-ECA times, 81 ECA-SESA times, and 74 ECA-NO-SESA times. Thus, 91% of SESA times are also SESA-ECA times (and the remaining 9% are SESA-NO-ECA times), and 52% of ECA times are ECA-SESA times (i.e., slightly more than half of all strong rainfall events at ECA occur with preceding strong events at SESA). During SESA-ECA
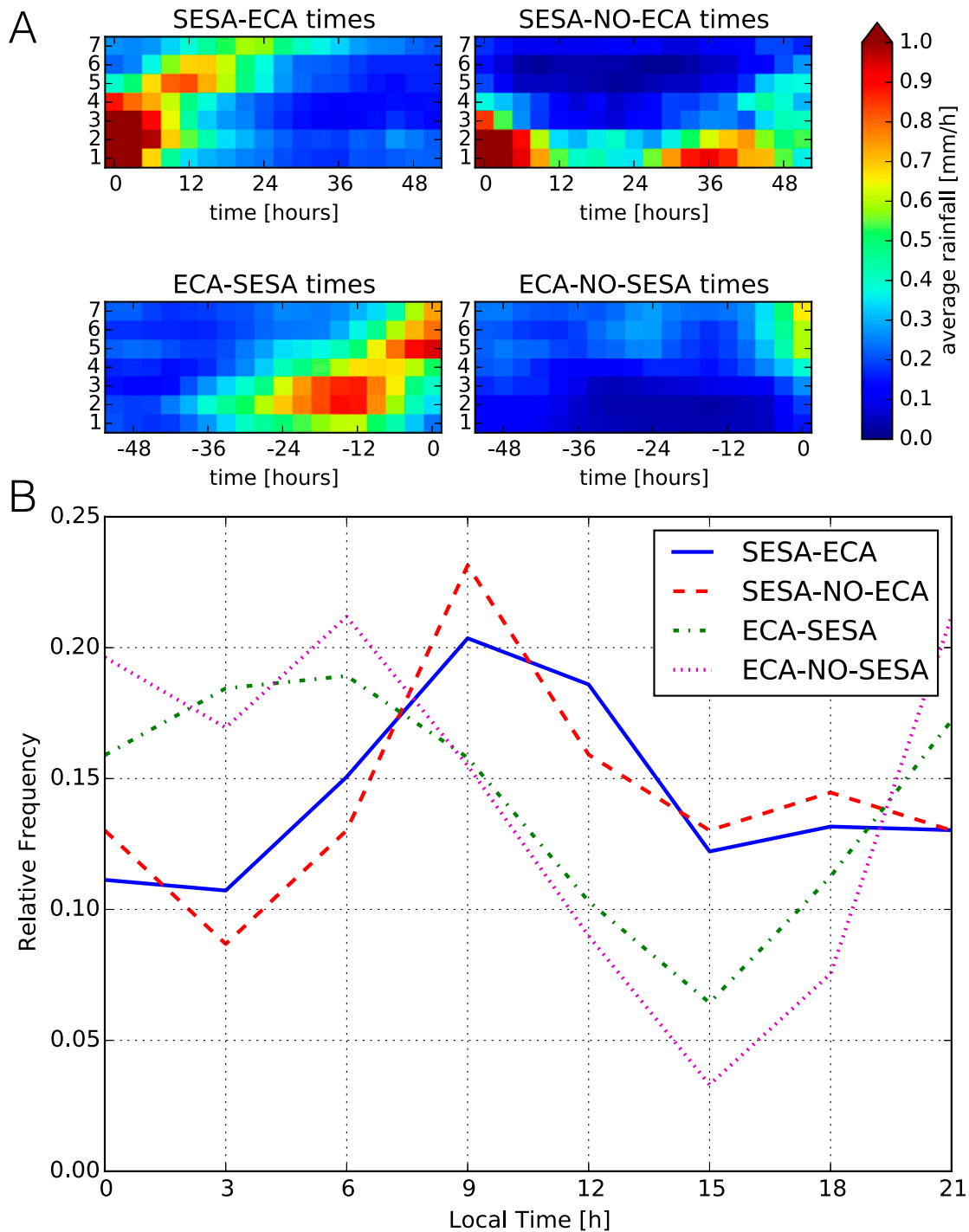
FIG. 2. (a) Spatially averaged rainfall over each of the seven boxes in Fig. 1 for each of the four different temporal subsets defined in the text. Time 0 corresponds to the time of peak rainfall in (top) SESA and (bottom) ECA. (b) Relative frequencies of the occurrence times in the diurnal cycle of the four temporal subsets. The 3-hourly rainfall rates are plotted at their midpoint: for example, values at 12 h are integrated from 1030 to 1330 local time.

and ECA-SESA times, rainfall indeed propagates along the sequence of seven spatial boxes, while this is not the case for SESA-NO-ECA and ECA-NO-SESA times (Fig. 2a). More than 50% of SESA-ECA times occur between 6 and 12 h, while more than

70% of ECA-SESA times occur between 21 and 9 h (Fig. 2b).

To understand the importance of the above regimes for the climatological rainfall budget, we computed the following rainfall fractions: SESA-ECA times account
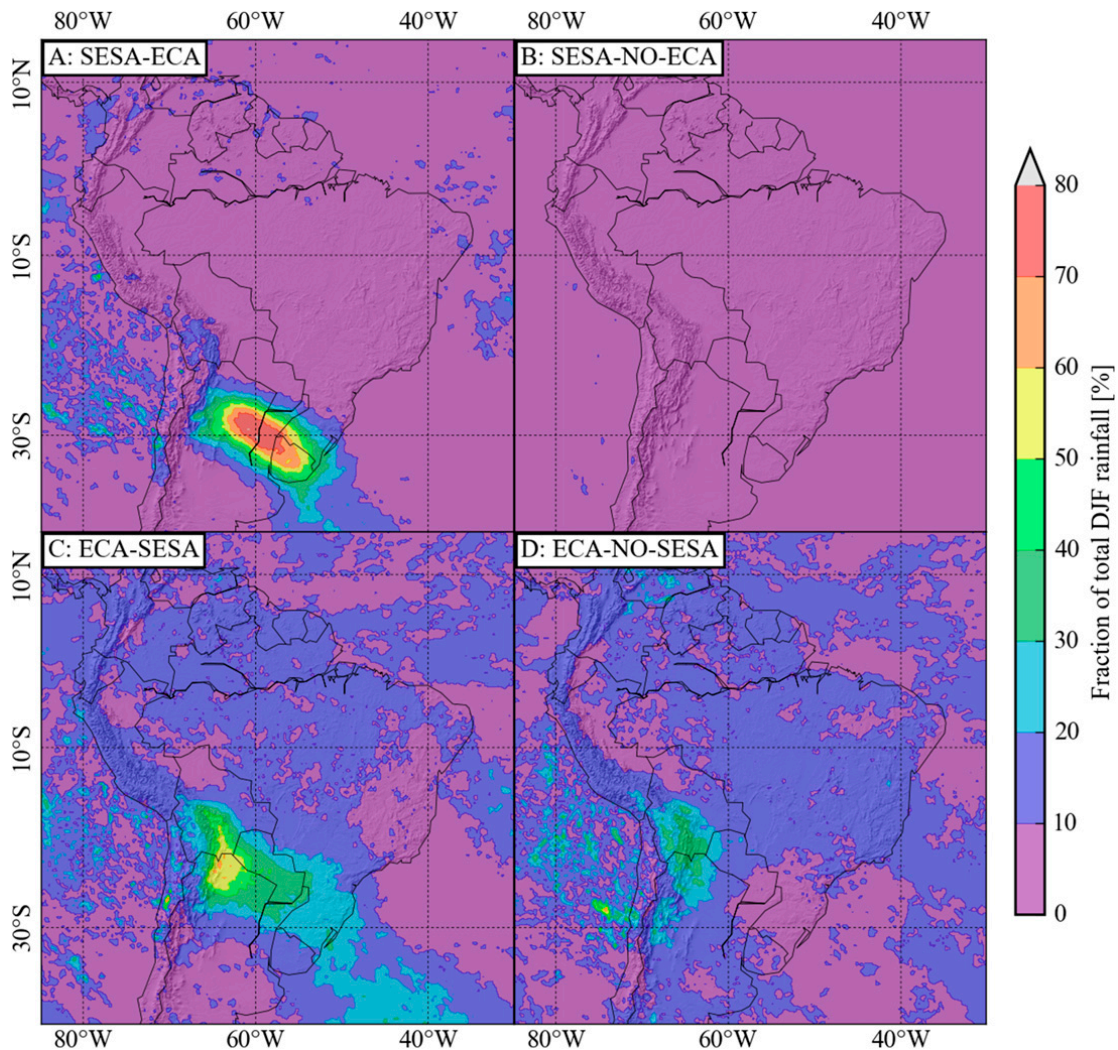
FIG. 3. Fraction of total seasonal rainfall in DJF accounted for during (a) SESA-ECA, (b) SESA-NO-ECA, (c) ECA-SESA, and (d) ECA-NO-SESA times.

for more than 70% of total DJF rainfall in SESA (Fig. 3a), and ECA-SESA times account for up to 60% of total DJF rainfall at the ECA (Fig. 3b). We note that the values shown slightly differ from the ones we found in Boers et al. (2014a) because of the different selection criteria based on averaging rainfall over the different SESA and ECA boxes employed here. For comparison, less than 10% of total DJF rainfall in SESA occurred during SESA-NO-ECA times, and less than 40% of total DJF rainfall in ECA occurs during ECA-NO-SESA times.

Composites of rainfall and geopotential height and wind fields at 850 hPa centered at the time of strong rainfall in SESA that will be followed (within 6–36 h) by strong rainfall at the ECA (SESA-ECA times; Fig. 4) show that already 2 days prior to peak rainfall in SESA, there exists a frontal system between 35° and 40°S. The associated low pressure anomaly reaches

northward along the eastern slopes of the southern Andes in the form of a tongue, which develops when the frontal systems' low pressure anomaly merges with the NAL (Arraut and Barbosa 2009). This tongue deepens and propagates farther north during the subsequent 24 h (from −48 to −24 h), with strong winds from the tropics approximately following its isobars. Around −12 h, a part of the South Pacific high begins to cross the southern Andes, leading to relatively high pressure immediately east of the Andean slopes around 35°S. This results in the formation of a saddle point of the isobars at 35°S, 65°W, at which cold and dry winds from the south meet with moist and warm winds from the tropics. This leads to strong frontogenesis in equivalent potential temperature, which is mainly caused by deformation of the wind field (Arraut and Barbosa 2009). Rainfall in SESA starts exactly at the position of this saddle point (i.e., the deformation axis) and will
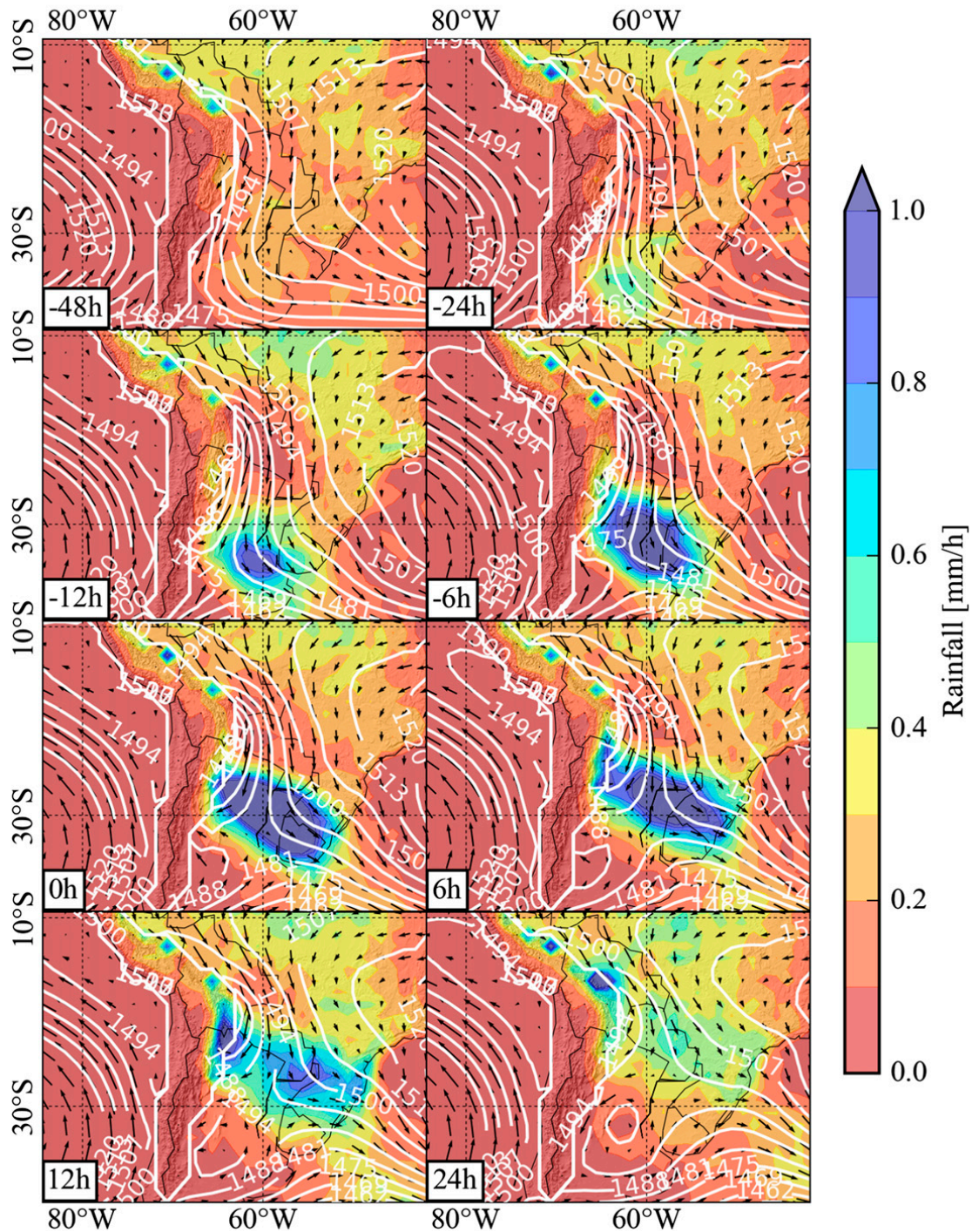
SESA-ECA: Rainfall, 850mbar GPH and Winds

FIG. 4. Composites of rainfall (color), geopotential height (m; contours), and wind fields (vectors) at 850 hPa from 48 h before to 24 h after SESA-ECA times. The label 0 h corresponds to the time when rainfall peaks in SESA. Rainfall values are derived from the TRMM 3B42 V7 dataset, while the remaining variables are obtained from the MERRA dataset.

propagate farther according to its position during the next 24 h (lags −12 h to +12 h). After rainfall in SESA reached its maximum at 0 h, high rainfall can be observed northeastward toward Paraguay and southern Brazil, but we also observe strong rainfall propagating northwestward toward the central Andes, reaching up to 16°S at the ECA.

For SESA-NO-ECA times (Fig. 5), composites also show such a low pressure tongue and the frontal system

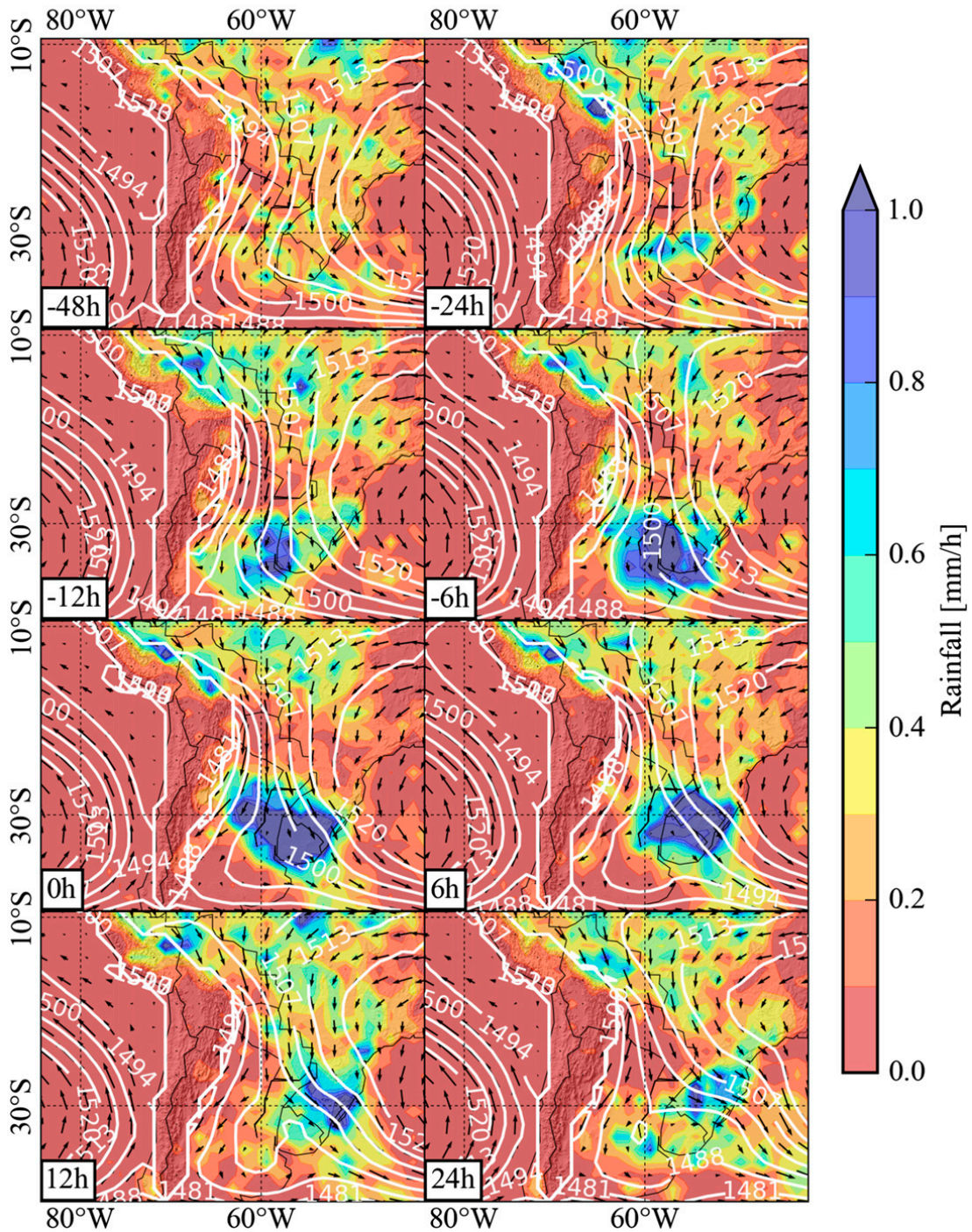## SESA-NO-ECA: Rainfall, 850mbar GPH and Winds

FIG. 5. As in Fig. 4, but for SESA-NO-ECA times.

moving northeastward, but the isobar saddle point never goes farther north than 35°S, 65°W. At 0 h, there is abundant rainfall in SESA, which will subsequently move northeastward in the subsequent time steps, but no rainfall occurs to the west at the slopes of the Andes. Despite the low pressure tongue, wind speeds east of the

Bolivian Andes are lower at 0 h as compared to SESA-ECA times.

Composites centered at times of strong rainfall at the ECA that were preceded (within 6–36 h) by strong rainfall in SESA (ECA-SESA times; Fig. 6) reveal that the isobar saddle point already developed around 35°S,
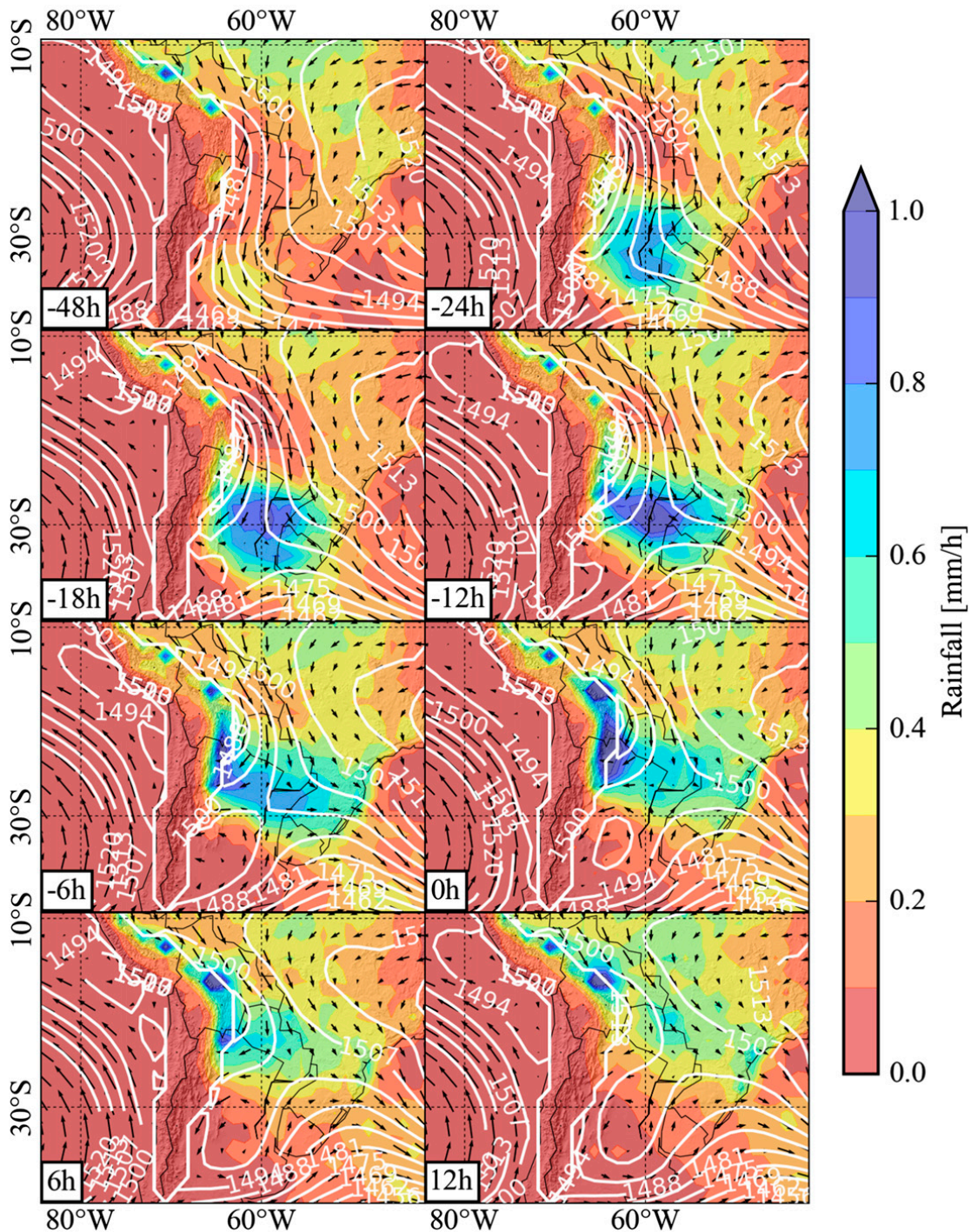
ECA-SESA: Rainfall, 850mbar GPH and Winds

FIG. 6. Composites of rainfall (color), geopotential height (m; contours), and wind fields (vectors) at 850 hPa from 48 h before to 12 h after ECA-SESA times. In contrast to Fig. 4, in this figure the label 0 h corresponds to the time when rainfall peaks at the ECA. Since the temporal delays between events at SESA and ECA are not constant, the composites for ECA-SESA times shown in this figure are not simply shifted composites for SESA-ECA times.

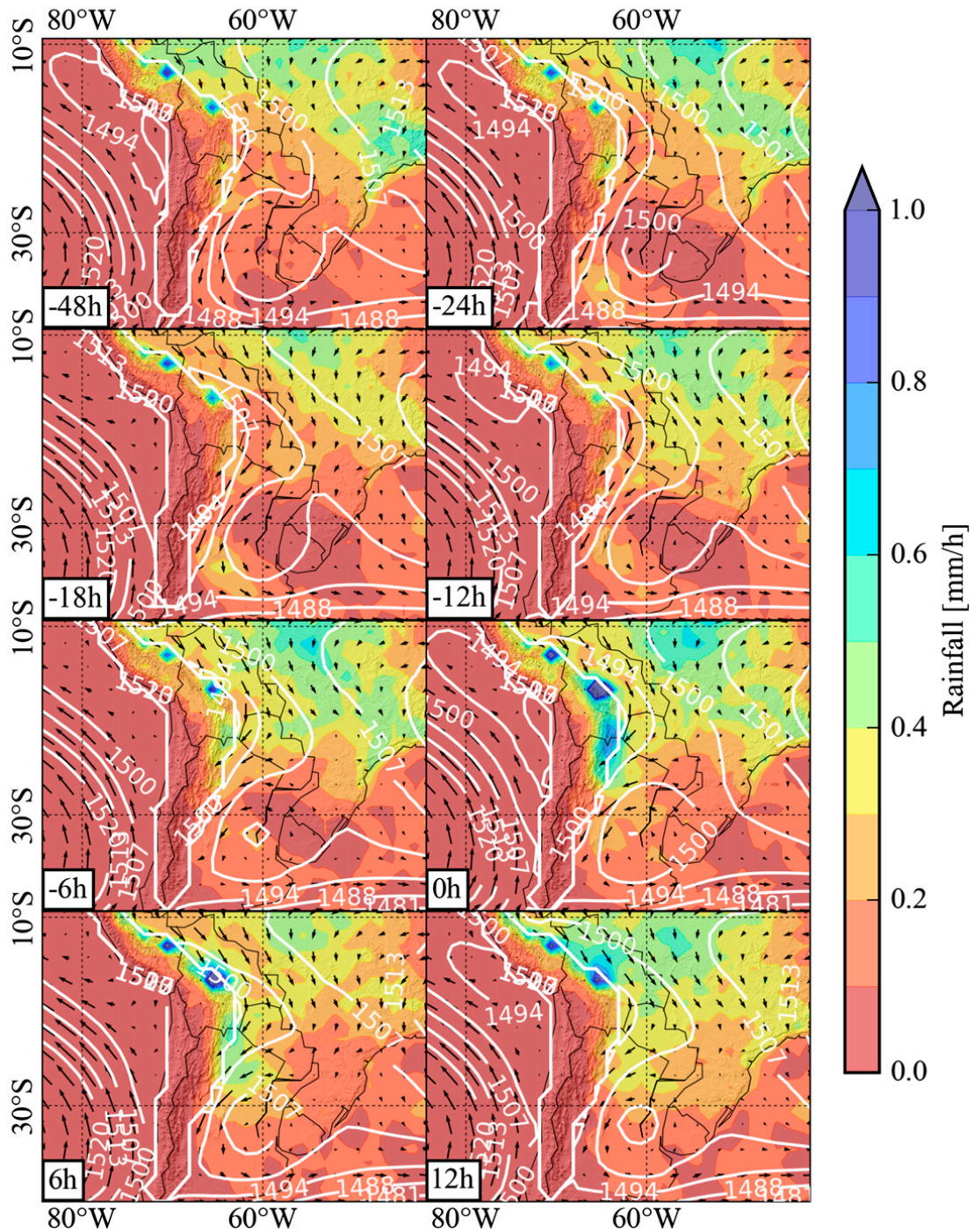## ECA-NO-SESA: Rainfall, 850mbar GPH and Winds

FIG. 7. As in Fig. 6, but for ECA-NO-SESA times.

65°W at −48 h relative to the time of rainfall at the ECA. During the following time steps, the isobaric saddle point will move northeastward together with the frontal system. Strong rainfall in SESA starts (−24 h) where the saddle point promotes deformation and thus fronto-genesis. At 0 h, the saddle point moved farther north,

and the position where southerly and northerly winds meet is shifted toward the ECA, where strong rainfall can be observed during the subsequent 12 h.

For ECA-NO-SESA (Fig. 7) times, there is no frontal system and no low pressure anomaly approaching SESA from the south. Instead, a high pressure cell persists over
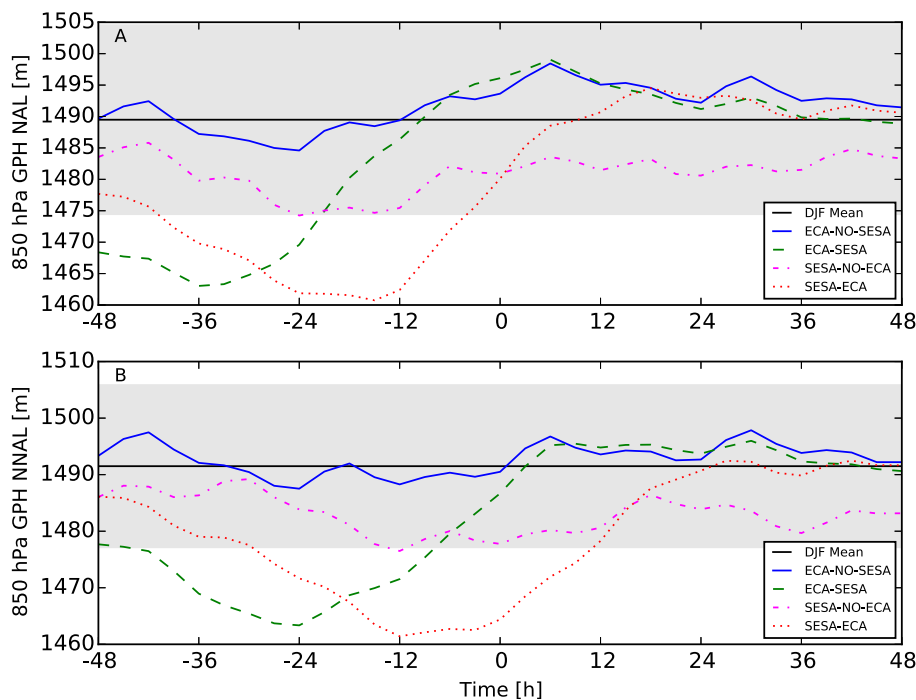
FIG. 8. (a) Mean geopotential height and standard deviations at 850 hPa over the climatological position of the NAL, represented by a box defined by 32°S, 68°W and 27°S, 65°W. Composites are shown for the four climatic regimes SESA-ECA, SESA-NO-ECA, ECA-SESA, and ECA-NO-SESA, as well as for DJF climatology. Shaded areas correspond to one standard deviation. (b) The same for the region NNAL, represented by a box defined by 25°S, 66°W and 20°S, 63°W.

SESA for the entire composite period. Rainfall at the ECA at 0 h is more pronounced in the northern part of ECA than in the southern part as compared to ECA-SESA times.

b. Variability of the northwestern Argentinean low

In this section, we give a quantitative analysis of the variability of geopotential height and wind fields at two different locations in the vicinity of the NAL.

At the climatological position of the NAL [defined by 32°S, 68°W and 27°S, 65°W, following Seluchi and Saulo (2003); see Fig. 1], geopotential height at 850 hPa begins to decrease already 2 days prior to SESA-ECA times and reaches its minimum value within this time span between 15 and 12 h prior to SESA-ECA times (Fig. 8a). For ECA-SESA times, the local minimum is already reached 36 h before peak rainfall in ECA. Both exceed the one standard deviation band during these times. For SESA-NO-ECA and ECA-NO-SESA times, no such clear variation can be observed.

For the region north of the NAL (NNAL; defined by 25°S, 66°W and 20°S, 63°W, close to box 6 in Fig. 1), geopotential height at 850 hPa shows a qualitatively similar behavior (Fig. 8b), but the local minimum is assumed to be shorter before SESA-ECA and ECA-SESA times (i.e., later in absolute time): For SESA-ECA

times, the minimum is located 12 h before, and for ECA-SESA times, 24 h before. Geopotential height does not leave the one standard deviation band of DJF climatology for SESA-NO-ECA and ECA-NO-SESA times.

The meridional components of 850-hPa winds averaged over the regions NAL and NNAL show significant patterns corresponding to the propagation of strong rainfall events (Fig. 9): For NAL and SESA-ECA times, the meridional component decreases in absolute terms in the 36 h before rainfall in SESA, crosses the DJF mean of $-4.1\,\mathrm{m\,s^{-1}}$ at 21 h prior, reaches its lowest absolute value ($0\,\mathrm{m\,s^{-1}}$) at the time of rainfall in SESA, and decreases thereafter. For ECA-SESA times, the behavior is similar, but the maximum is reached 12 h before rainfall at the ECA. At NNAL, for SESA-ECA and for ECA-SESA times, the northerly component is more pronounced than at NAL before rainfall at SESA and ECA, respectively. In addition, the maximum values are reached later: almost 24 h after rainfall in SESA for SESA-ECA times and 9 h later than rainfall at ECA for ECA-SESA times.

c. Connection to the low-level jet east of the Andes

The composite wind fields (Figs. 4, 5, 6, and 7) suggest a possible role of the SALLJ in the propagation of strong rainfall cells from SESA to ECA.
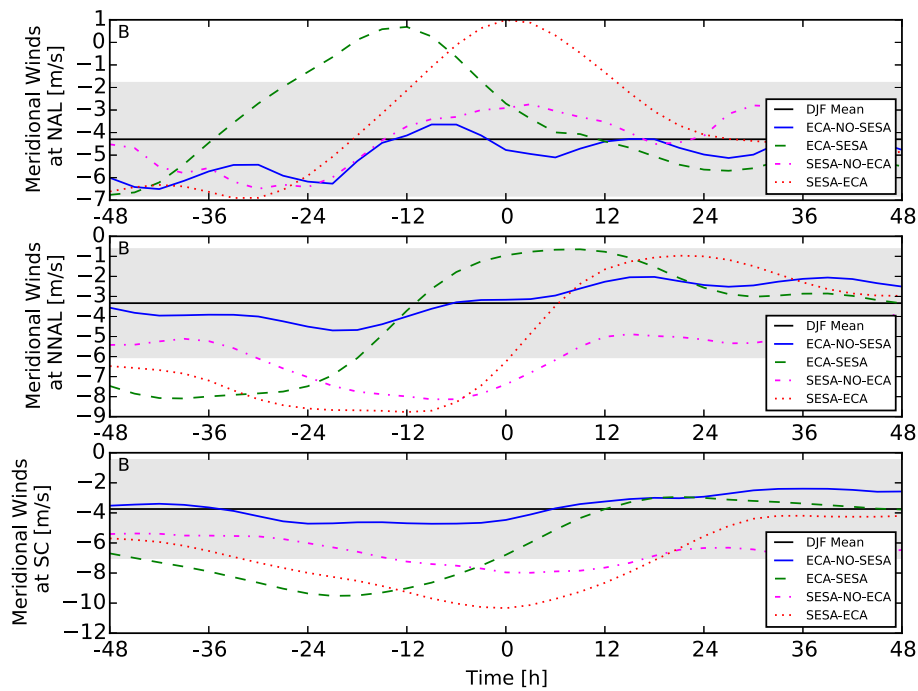
FIG. 9. Composite meridional wind speeds at 850 hPa over the climatological position of the NAL, represented by a box defined by 32°S, 68°W and 27°S, 65°W, for the spatial box NNAL, defined by 25°S, 66°W and 20°S, 63°W, as well as for SC (17°S, 62°W). Composites are shown for the four climatic regimes SESA-ECA, SESA-NO-ECA, ECA-SESA, and ECA-NO-SESA, as well as for the DJF climatology. Shaded areas correspond to one standard deviation of the DJF climatology.

Meridional wind speeds at Santa Cruz de la Sierra in Bolivia (Fig. 9) for SESA-ECA times begin to increase already 2 days prior and reach their maximum exactly at the time of strong rainfall at SESA. At this time, meridional wind speeds differ by more than one standard deviation from the DJF mean, and—even on average—meet the criterion for SALLJ events of absolute wind speeds larger than $12\,m\,s^{-1}$ (not shown). Meridional wind speeds also increase prior to ECA-SESA times but already reach their maximum about one day before strong rainfall occurs at the ECA.

The fraction of SALLJ times that are also SESA times increases when more restrictive SALLJ conditions are chosen (wind speeds at Santa Cruz from 9 to $18\,m\,s^{-1}$). The same holds true for SALLJ times that are also SESA-ECA times, but not for SALLJ times that are also SESA-NO-ECA times, for which no trend can be observed (Fig. 10a). Furthermore, rainfall at SESA has a positive trend with stronger SALLJ conditions for SALLJ times that are also SESA or SESA-ECA times (Fig. 10b). By implication, wind speeds at Santa Cruz increase with more restrictive SALLJ conditions (Fig. 10c). Similarly, the fraction of SALLJ times that are also ECA times increases when choosing a more restrictive SALLJ condition. While the same qualitative behavior is shown for SALLJ times that are also ECA-SESA times, for ECA-NO-SESA

times, the fraction of SALLJ times decreases for stronger LLJ conditions (Fig. 10d). Rainfall at the ECA seems to be independent of the SALLJ condition (Fig. 10e). Again, by implication, wind speeds at Santa Cruz increase with more restrictive SALLJ conditions (Fig. 10f). For all SALLJ conditions ($9–18\,m\,s^{-1}$), the fraction of SESA-ECA (ECA-SESA) times that are SALLJ times as well is higher than the fraction of SESA-NO-ECA (ECA-NO-SESA) times (Figs. 10g,j) that are SALLJ times.

6. Discussion

a. Composites for the four regimes

The propagation of strong and spatially extensive rainfall events from SESA to ECA is a recurring feature of the monsoon season, with more than 90% of strong rainfall events in SESA propagating upstream (of the low-level moisture flow) toward the ECA, leading to strong rainfall there within the subsequent 6–36 h. This climatic regime is responsible for more than 70% (50%) of total DJF rainfall at SESA (ECA) and thus provides a large contribution to the total water supply in the area but also imposes a great risk to the resident population in the form of floods and landslides (Bookhagen and Strecker 2012; Boers et al. 2014a).
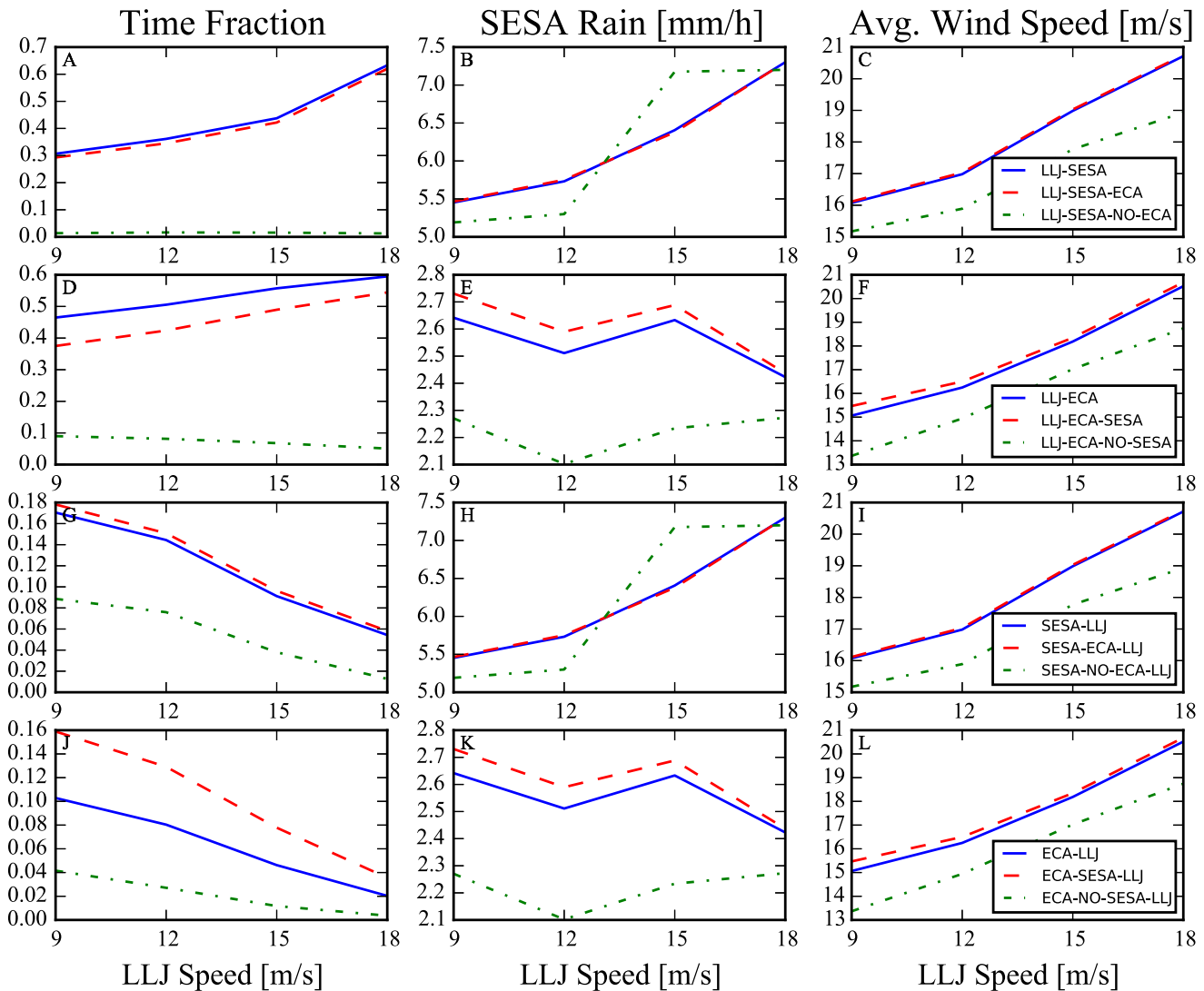
FIG. 10. Connection between the SALLJ and the propagation events of strong rainfall from SESA to ECA. (a) Fractions of SALLJ times that are also SESA (solid blue), SESA-ECA (red dashed), and SESA-NO-ECA (green dotted–dashed) times for LLJ speed criteria from 9 to 18 m s^{-1}. (b) Spatially averaged rainfall in SESA during the respective times. (c) Average wind speeds at 850 hPa at Santa Cruz de la Sierra (17°S, 62°W) for the respective times. (d)–(l) The equivalent information, but for different temporal subsets, as indicated by the color legends in the right column, which apply to all of the respective row.

Comparing the composites for SESA-ECA times ([Fig. 4](#)) and SESA-NO-ECA times ([Fig. 5](#)), we infer that initial rainfall in SESA will propagate to the ECA if a saddle point of the isobars develops at 35°S, 65°W, connecting the NAL with a midlatitude low pressure cell approaching from the south. This saddle point causes deformation and, hence, frontogenesis, which in turn provides favorable conditions for organized convection. The midlatitude low pressure cell is itself embedded on an eastward-moving Rossby wave train that originates from the western Pacific Ocean. The impacts of this wave train on South American convection have, for instance, been studied in ([Renwick and Revell 1999](#); [Díaz and Aceituno 2003](#)). It can be detected from the geopotential

height and wind anomalies at 850 and 250 hPa composited for SESA-ECA times ([Figs. 11](#) and [12](#)).

Without the topological feature of a saddle point of the isobars (SESA-NO-ECA times), there still occurs abundant rainfall in SESA because of the cold front, but rain will only propagate northeastward. On the other hand, if the saddle point is present (SESA-ECA times), it will cause a clash of cold and dry winds from the south with warm and moist winds from the tropics: A high pressure cell crossing the southern Andes (the southwestern part of the saddle point) in the aftermath of the preceding low pressure will drive cold air masses from the south toward the slopes of the Andes, where they meet warm and moist air masses originating from the
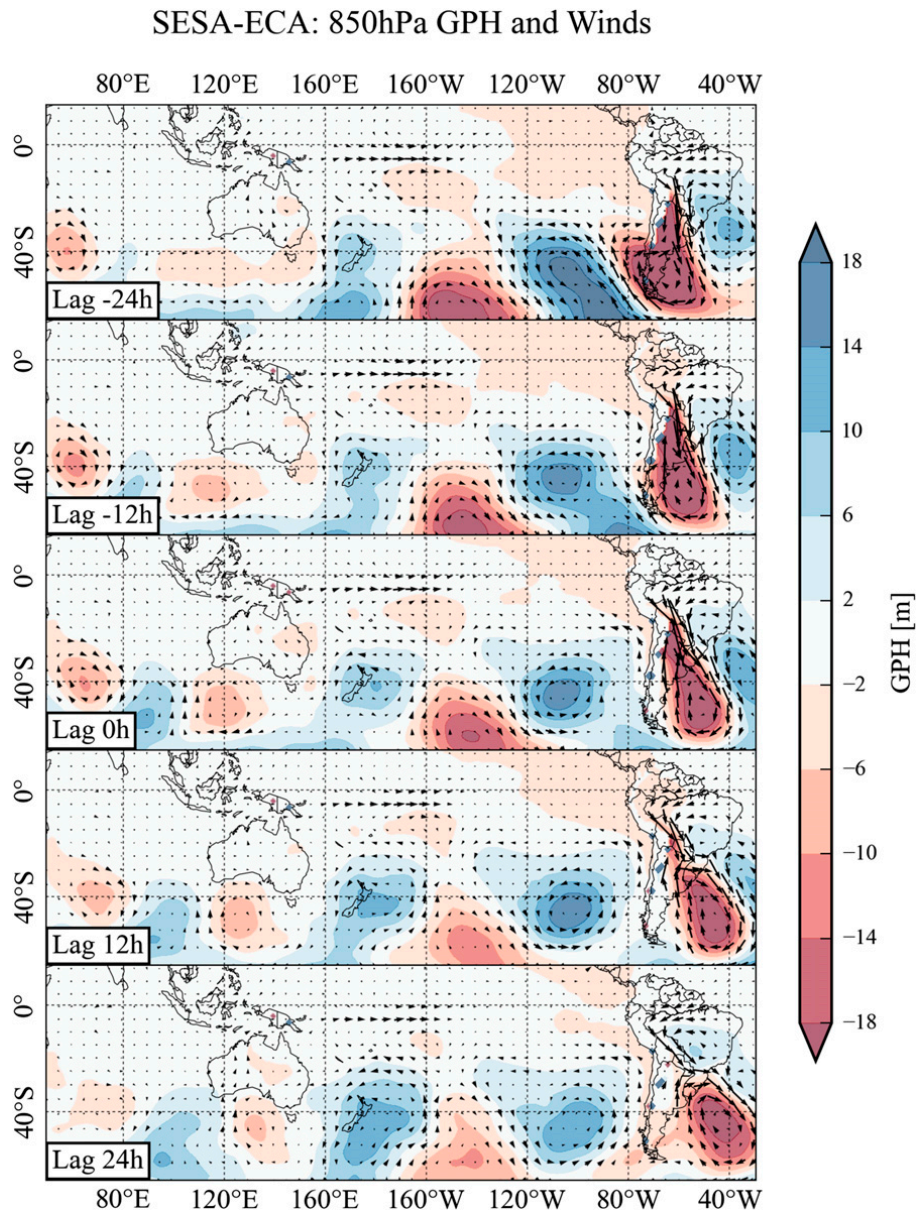
SESA-ECA: 850hPa GPH and Winds

FIG. 11. Composite anomalies vs DJF climatology of 850-hPa geopotential height and wind fields for 1 day before to 1 day after SESA-ECA times. Note the eastward-moving oscillation of negative and positive pressure anomalies over the southeastern Pacific and how the low pressure cell over the southern tip of South America merged with the NAL before retreating toward the subtropical Atlantic Ocean. Regions of nonsignificant anomalies based on a one-sample-location *t* test are shown in white.

Amazon to cause abundant rainfall in the southern parts of the ECA. Because of the eastward movement of the Rossby wave train, the high pressure cell pushes the saddle point and thus the deformation axis of fronto-genesis northwestward in the subsequent time steps, explaining the northwestward propagation of the convective development and, hence, precipitation. It should be noted, however, that this does not imply that single MCS propagate northeastward, but rather that the conditions favoring convective development propagate

in this direction and cause the formation of serial MCS along the way, as has also been described in the case study by Anabor et al. (2008).

At the same time, the preceding deepening of the low pressure tongue leads to an increase of northerly wind speeds east of the Andes, in particular in northern Bolivia, enhancing the moisture flow from the tropics. These strengthened winds lead to strong rainfall peaks in the northern parts of the ECA because of orographic lifting (Bookhagen and Strecker 2008). The presence of
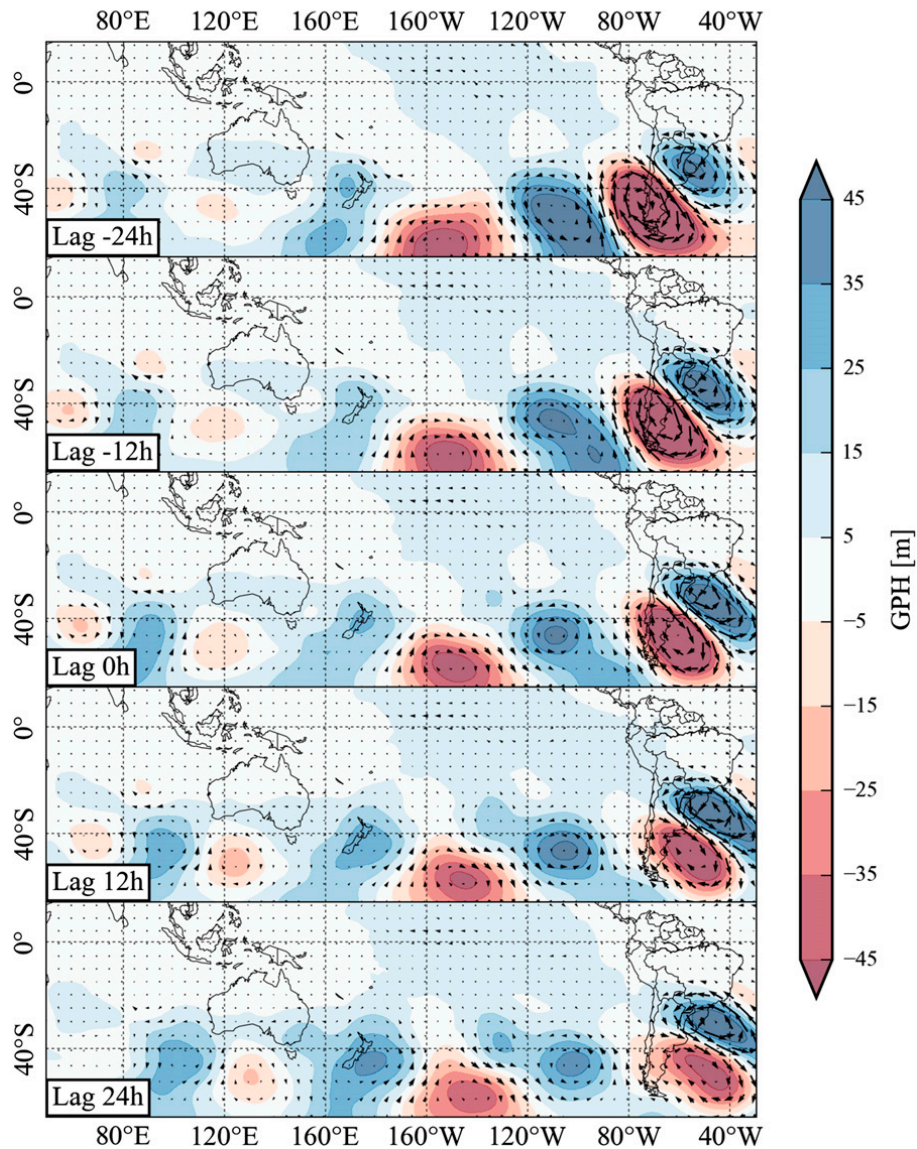
SESA-ECA: 250hPa GPH and Winds

FIG. 12. Composite anomalies vs DJF climatology of 250-hPa geopotential height and wind fields for 1 day before to 1 day after SESA-ECA times. Note the eastward-moving Rossby wave train over the southern Pacific Ocean. Regions of nonsignificant anomalies based on a one-sample-location *t* test are shown in white.

the NAL is thus a necessary condition for the propagation of convective activity from SESA to ECA. During the summer season, the NAL is mainly thermally driven, although a strengthening effect caused by the Zonda winds cannot be ruled out, which are however more relevant during the winter season (Seluchi and Saulo 2003). In (Garreaud 2009), the author describes the Zonda winds as a consequence of the interplay of the surface low and strong upper-level westerlies crossing the Andes, although a previous intensification of the low east of the subtropical Andes is also suggested because

of leeside subsidence of warm air, hinting at a possible feedback mechanism.

As expected, composites for ECA-SESA times yield qualitatively very similar results as composites for SESA-ECA times (shifted by about 1 day). On the other hand, composites for ECA-NO-SESA times show the average atmospheric conditions for strong rainfall events that were not preceded by rainfall at SESA. Although these times account for more than 30% of DJF rainfall in parts of the ECA, comparing composites of ECA-SESA times with composites of ECA-NO-SESA

times reveals that, for ECA-NO-SESA times, rainfall is confined toward the north, where orographic lifting should play a more important role because of the typical direction of low-level winds in relation to the orientation of the Andes. Thus, these strong rainfall events at the ECA are not due to the discussed mechanism, but rather a direct consequence of orographic effects in these parts of ECA.

b. Variability of the northwestern Argentinean low

The deepening of the NAL around 24 h before rainfall peaks at SESA and 36 h before rainfall peaks at ECA (Fig. 8) implies that this low pressure system plays a crucial role for modulating the propagation of rainfall clusters from SESA to the ECA. This is consistent with the discussion above, since a deep NAL is necessary for the formation of the described saddle point of isobars. The role of the NAL in this situation is twofold: First, it enhances the speed of warm and moist low-level winds from the north, establishing conditions favoring the establishment of the Chaco jet (Saulo et al. 2004). Second, in interplay with the high pressure cell approaching from the west and crossing the Andes south of the NAL, it causes cold westerly winds to the south to tilt counterclockwise, resulting in very small values of the typically southward-directed meridional low-level flow at NAL (Fig. 9).

In Garreaud and Wallace (1998) and Garreaud (2000) it has been suggested that northward-directed low-level winds are pushing the convective activity northward. However, in our high-temporal-resolution composites, absolute winds do not point northward after crossing 28°S for SESA-ECA times (cf. the meridional component at NAL and NNAL for SESA-ECA times). Instead, dictated by the saddle point, southerly and northerly winds meet at the climatological location of the NAL, with a pronounced positive meridional anomaly, indicating that the typically northerly winds slow down significantly during these times (Figs. 9 and 6 at 0 h). Therefore, we propose that the propagation of strong rainfall from SESA to ECA occurs for two reasons: first, the deformation of the flow around the saddle point where cold dry air masses from the South collide with moist warm air masses from the tropics, leading to strong frontogenesis in equivalent potential temperature and, second, the westward lifting of the air masses over the sloping terrain (orographic forcing).

c. Connection to the low-level jet east of the Andes

There exists an obvious connection between the propagation of strong rainfall from SESA to ECA and the SALLJ, as determined from wind speeds at Santa Cruz (Fig. 9). In particular, the increase in fractions of SALLJ times that are also SESA-ECA or ECA-SESA times with increasing wind speeds (Figs. 10a,b) suggests that, the faster the winds, the higher the probability of a rainfall propagating from SESA to ECA. This is consistent with the discussion above, since stronger winds from the tropics enhance the deformation at the saddle point. However, despite the increase of fractions of SALLJ times that are also SESA-ECA (or ECA-SESA) times when choosing stronger SALLJ conditions, during more than half of the times that are SALLJ events according to the most common definition [$12\,m\,s^{-1}$; Marengo et al. (2004); Salio et al. (2007)], rainfall does not propagate from SESA to ECA. Similarly, only 15% (13%) of SESA-ECA (ECA-SESA) times are SALLJ times (Figs. 10g,j, determined using the 12-$m\,s^{-1}$ condition). Therefore, we emphasize that the SALLJ and the propagation of atmospheric conditions favoring convection from SESA to ECA are neither necessary nor sufficient conditions for one another.

The physical mechanism described above suggests that increased wind speeds at Santa Cruz (and associated SALLJ events) are a passive consequence of the formation of the low pressure tongue developing when the NAL joins the low pressure system of the northward-propagating cold front. This is supported by the fact that the maximum southward wind speed at Santa Cruz is assumed at the time when front-induced rainfall in SESA reaches its maximum (Fig. 9). Furthermore, the deeper the NAL, the stronger is the pressure gradient, and thus the faster the winds along the isobars. On the other hand, the deeper the NAL, the more likely is the development of the low pressure tongue and the associated saddle point of the isobars, and therefore the more likely it is that rainfall will propagate from SESA to ECA. Therefore, we argue that the deepening of the low pressure tongue acts as common cause for increased wind speeds at Santa Cruz and increased deformation and, hence, frontogenesis at the saddle point, which in turn leads to the propagation of strong rainfall from SESA to ECA. In turn, this also suggests that the moisture inflow from the tropics (e.g., by the SALLJ) is not an independent driver of rainfall in SESA or ECA. Thus, the positive relationship between the strength of the low-level flow from the Amazon along the Andes toward the subtropics and rainfall in the subtropics, which was, for example, observed in Salio et al. (2007) and in Arraut et al. (2012) using monthly data, is not due to a direct causal relationship. Instead, it is due to the frontal system approaching from the south and its interplay with the NAL as common drivers.

Since we consider only strong rainfall events during DJF (above the 90th percentile), it seems likely that most of the considered rainfall events are caused by

MCS (Durkee and Mote 2009; Durkee et al. 2009; Boers et al. 2013, 2015). Anabor et al. (2008) studied particular cases of serial MCS that develop subsequently from SESA toward the northwestern Argentinean Andes. In fact, all three serial MCS events analyzed in that study, which occurred during DJF on 5 December 2005, 12 January 2006, and 16 January 2006, fall into our SESA-ECA times. Recalling that more than 90% of strong rainfall events in SESA will be followed by strong events at the ECA, our study suggests that these serial MCS might be less exotic than previously thought and may play a crucial role for total DJF rainfall amounts as well as any natural hazards they might lead to. Therefore, it seems plausible that these MCS typically develop in association with midlatitude low pressure systems and corresponding frontal systems approaching from the south and crossing SESA: The moisture needed for such a northwestward propagation of subsequent organized convection is provided by the low-level flow from the Amazon. However, the mechanism actually triggering the propagation of conditions favoring convection is the interplay of the midlatitude low pressure systems approaching from the south with the NAL and the orientation of the Andes mountain range. This interplay leads to the formation of a saddle point in pressure levels, which causes pronounced frontogenesis through deformation, providing the environment for the development of the MCS. Because of the eastward movement of the Rossby wave train on which these lows are embedded, the saddle point is pushed northward by the next high pressure cell approaching from the west. This explains the propagation of atmospheric conditions favoring convection from SESA toward the ECA. The rather periodic occurrence of this phenomenon can be furthermore explained by the periodicity of the midlatitude wave train. In addition, we speculate that the variability of NAL indirectly responds to the alternation of low and high pressure systems in a way that enhances the overall mechanism: suppressed convection in the aftermath of a propagating thunderstorm will favor the subsequent thermal deepening of the NAL once again, which in turn prepares the conditions for the next occurrence of the saddle point in the pressure configuration.

7. Conclusions

We have shown that the propagation of strong rainfall associated with deep convection from southeastern South America toward the eastern slopes of the central Andes is a rather typical feature of the South American monsoon system. Based on high-spatiotemporal-resolution data, we have described and discussed a climatic mechanism that, in accordance with corresponding composites,

explains this propagation. This mechanism consists of an interplay of low-level moisture flow from the tropics, alternating low and high pressure cells originating from midlatitudes, and the Andean orography. The interplay of these features leads to the formation of a saddle point of the pressure levels, where deformation leads to strong frontogenesis.

The results of our systematic study are consistent with case studies on the propagation of conditions favoring organized deep convection from southeastern South America to the eastern central Andes. Although it seems plausible, based on surface rainfall estimates provided by the TRMM 3B42 V7 dataset alone, we cannot prove that the propagation events of strong rainfall we identified are exclusively due to organized convective systems. In view of the complexity of the physics behind the formation of organized convection (see, e.g., Lima and Wilson 2008), this will be the subject of future work.

Our key findings can be summarized as follow:

(i) The propagation of rainfall toward the central Andes only occurs if a midlatitude low merges with a previously established thermal low in northwestern Argentina such that a saddle point establishes in the pressure configuration. Abundant rainfall will occur at the position of this saddle point because of the deformation and associated frontogenesis around this saddle point, causing clashes of cold and dry air from the south with warm and moist air from the north.

(ii) Because of the eastward movement of the Rossby wave train that dictates the occurrence of the midlatitude low and the blocking effect of the subsequent midlatitude high, this saddle point and hence the conditions favoring deep convection move northwestward toward the central Andes, where the associated rainfall is further enhanced by orographic lifting effects.

(iii) The South American low-level jet east of the Andes is neither a necessary nor a sufficient condition for their formation. Instead, it can be seen as a consequence of the described atmospheric mechanism, since the low-level wind channel along the isobars of the merged low pressure cells may sometimes be pronounced enough to meet the criterions of a low-level jet.

(iv) The low-level wind channel conveying tropical moisture along the Andean slopes to the South American subtropics provides the conditions necessary for the formation of convective systems but does not itself initiate their onset. Instead, the formation of the saddle point should be viewed as a common driver for the establishment of this

wind channel and the occurrence of these large rainfall clusters.

REFERENCES

Anabor, V., D. J. Stensrud, and O. L. L. de Moraes, 2008: Serial upstream-propagating mesoscale convective system events over southeastern South America. *Mon. Wea. Rev.*, **136**, 3087–3105, doi:10.1175/2007MWR2334.1.

Arraut, J. M., and H. M. J. Barbosa, 2009: Large scale features associated with strong frontogenesis in equivalent potential temperature in the South American subtropics east of the Andes. *Adv. Geosci.*, **22**, 73–78, doi:10.5194/adgeo-22-73-2009.

——, C. Nobre, H. M. J. Barbosa, G. Obregon, and J. Marengo, 2012: Aerial rivers and lakes: Looking at large-scale moisture transport and its relation to Amazonia and to subtropical rainfall in South America. *J. Climate*, **25**, 543–556, doi:10.1175/2011JCLI4189.1.

Berbery, E. H., and E. A. Collini, 2000: Springtime precipitation and water vapor flux over southeastern South America. *Mon. Wea. Rev.*, **128**, 1328–1346, doi:10.1175/1520-0493(2000)128<1328:SPAWVF>2.0.CO;2.

Boers, N., B. Bookhagen, N. Marwan, J. Kurths, and J. Marengo, 2013: Complex networks identify spatial patterns of extreme rainfall events of the South American monsoon system. *Geophys. Res. Lett.*, **40**, 4386–4392, doi:10.1002/grl.50681.

——, ——, H. M. J. Barbosa, N. Marwan, J. Kurths, and J. Marengo, 2014a: Prediction of extreme floods in the eastern central Andes based on a complex network approach. *Nat. Commun.*, **5**, 5199, doi:10.1038/ncomms6199.

——, A. Rheinwalt, B. Bookhagen, H. M. J. Barbosa, N. Marwan, J. A. Marengo, and J. Kurths, 2014b: The South American rainfall dipole: A complex network analysis of extreme events. *Geophys. Res. Lett.*, **41**, 7397–8007, doi:10.1002/2014GL061829.

——, B. Bookhagen, J. Marengo, N. Marwan, J.-S. V. Sorch, and J. Kurths, 2015: Extreme rainfall of the South American monsoon system: A dataset comparison using complex networks. *J. Climate*, **28**, 1031–1056, doi:10.1175/JCLI-D-14-00340.1.

Bonner, W. D., 1968: Climatology of the low level jet. *Mon. Wea. Rev.*, **96**, 833–850, doi:10.1175/1520-0493(1968)096<0833:COTLLJ>2.0.CO;2.

Bookhagen, B., and M. R. Strecker, 2008: Orographic barriers, high-resolution TRMM rainfall, and relief variations along the eastern Andes. *Geophys. Res. Lett.*, **35**, L06403, doi:10.1029/2007GL032011.

——, and ——, 2012: Spatiotemporal trends in erosion rates across a pronounced rainfall gradient: Examples from the southern central Andes. *Earth Planet. Sci. Lett.*, **327–328**, 97–110, doi:10.1016/j.epsl.2012.02.005.

Byerle, L. A., and J. Paegle, 2002: Description of the seasonal cycle of low-level flows, flanking the Andes and their interannual variability. *Meteorologica*, **27**, 71–88.

Carvalho, L. M. V., C. Jones, and B. Liebmann, 2004: The South Atlantic convergence zone: Intensity, form, persistence, and relationships with intraseasonal to interannual activity and extreme rainfall. *J. Climate*, **17**, 88–108, doi:10.1175/1520-0442(2004)017<0088:TSACZI>2.0.CO;2.

——, A. E. Silva, C. Jones, B. Liebmann, P. L. Silva Dias, and H. R. Rocha, 2011: Moisture transport and intraseasonal variability in the South America monsoon system. *Climate Dyn.*, **36**, 1865–1880, doi:10.1007/s00382-010-0806-2.

Díaz, A., and P. Aceituno, 2003: Atmospheric circulation anomalies during episodes of enhanced and reduced convective cloudiness over Uruguay. *J. Climate*, **16**, 3171–3185, doi:10.1175/1520-0442(2003)016<3171:ACADEO>2.0.CO;2.

Durkee, J. D., and T. L. Mote, 2009: A climatology of warm-season mesoscale convective complexes in subtropical South America. *Int. J. Climatol.*, **30**, 418–431, doi:10.1002/joc.1893.

——, ——, and J. M. Shepherd, 2009: The contribution of mesoscale convective complexes to rainfall across subtropical South America. *J. Climate*, **22**, 4590–4605, doi:10.1175/2009JCLI2858.1.

Eltahir, E. A. B., and R. L. Bras, 1994: Precipitation recycling in the Amazon basin. *Quart. J. Roy. Meteor. Soc.*, **120**, 861–880, doi:10.1002/qj.49712051806.

Ferreira, R., T. Rickenbach, D. L. Herdies, and L. Carvalho, 2003: Variability of South American convective cloud systems and tropospheric circulation during January–March 1998 and 1999. *Mon. Wea. Rev.*, **131**, 961–973, doi:10.1175/1520-0493(2003)131<0961:VOSACC>2.0.CO;2.

Garreaud, R. D., 2000: Cold air incursions over subtropical South America: Mean structure and dynamics. *Mon. Wea. Rev.*, **128**, 2544–2559, doi:10.1175/1520-0493(2000)128<2544:CAIOSS>2.0.CO;2.

——, 2009: The Andes climate and weather. *Adv. Geosci.*, **22**, 3–11, doi:10.5194/adgeo-22-3-2009.

——, and J. M. Wallace, 1998: Summertime incursions of midlatitude air into subtropical and tropical South America. *Mon. Wea. Rev.*, **126**, 2713–2733, doi:10.1175/1520-0493(1998)126<2713:SIOMAI>2.0.CO;2.

Giovannettone, J. P., and A. P. Barros, 2009: Probing regional orographic controls of precipitation and cloudiness in the central Andes using satellite data. *J. Hydrometeor.*, **10**, 167–182, doi:10.1175/2008JHM973.1.

Huffman, G., and Coauthors, 2007: The TRMM Multisatellite Precipitation Analysis (TMPA): Quasi-global, multiyear, combined-sensor precipitation estimates at fine scales. *J. Hydrometeor.*, **8**, 38–55, doi:10.1175/JHM560.1.

Kiladis, G. N., and K. M. Weickmann, 1992: Extratropical forcing of tropical Pacific convection during northern winter. *Mon. Wea. Rev.*, **120**, 1924–1939, doi:10.1175/1520-0493(1992)120<1924:EFOTPC>2.0.CO;2.

Kousky, V. E., 1979: Frontal influences on northeast Brazil. *Mon. Wea. Rev.*, **107**, 1140–1153, doi:10.1175/1520-0493(1979)107<1140:FIONB>2.0.CO;2.

Lenters, J. D., and K. H. Cook, 1999: Summertime precipitation variability over South America: Role of the large-scale circulation. *Mon. Wea. Rev.*, **127**, 409–431, doi:10.1175/1520-0493(1999)127<0409:SPVOSA>2.0.CO;2.

Liebmann, B., and C. Mechoso, 2011: The South American monsoon system. *The Global Monsoon System: Research and Forecast*, World Scientific Series on Asia-Pacific Weather and Climate, Vol. 5, World Scientific, 137–157.

——, G. N. Kiladis, J. Marengo, T. Ambrizzi, and J. D. Glick, 1999: Submonthly convective variability over South America and

the South Atlantic convergence zone. *J. Climate*, **12**, 1877–1891, doi:10.1175/1520-0442(1999)012<1877:SCVOSA>2.0.CO;2.

——, ——, C. S. Vera, C. Saulo, and L. M. V. Carvalho, 2004: Subseasonal variations of rainfall in South America in the vicinity of the low-level jet east of the Andes and comparison to those in the South Atlantic convergence zone. *J. Climate*, **17**, 3829–3842, doi:10.1175/1520-0442(2004)017<3829:SVORIS>2.0.CO;2.

Lima, M. A., and J. W. Wilson, 2008: Convective storm initiation in a moist tropical environment. *Mon. Wea. Rev.*, **136**, 1847–1864, doi:10.1175/2007MWR2279.1.

Marengo, J. A., W. R. Soares, C. Saulo, and M. Nicolini, 2004: Climatology of the low-level jet east of the Andes as derived from the NCEP-NCAR reanalyses: Characteristics and temporal variability. *J. Climate*, **17**, 2261–2280, doi:10.1175/1520-0442(2004)017<2261:COTLJE>2.0.CO;2.

——, and Coauthors, 2012: Recent developments on the South American monsoon system. *Int. J. Climatol.*, **32**, 1–21, doi:10.1002/joc.2254.

Montes de Oca, I., 1995: Geografía y clima de Bolivia. *Bull. Inst. Fr. Etud. Andines*, **24**, 357–368.

Nicolini, M., A. C. Saulo, J. C. Torres, and P. Salio, 2002: Enhanced precipitation over southeastern South America related to strong low-level jet events during austral warm season. *Meteorologica*, **27**, 59–69.

Nogués-Paegle, J., and K. C. Mo, 1997: Alternating wet and dry conditions over South America during summer. *Mon. Wea. Rev.*, **125**, 279–291, doi:10.1175/1520-0493(1997)125<0279:AWADCO>2.0.CO;2.

Renwick, J., and M. Revell, 1999: Blocking over the South Pacific and Rossby wave propagation. *Mon. Wea. Rev.*, **127**, 2233–2247, doi:10.1175/1520-0493(1999)127<2233:BOTSPA>2.0.CO;2.

Rienecker, M. M., and Coauthors, 2011: MERRA: NASA's Modern-Era Retrospective Analysis for Research and Applications. *J. Climate*, **24**, 3624–3648, doi:10.1175/JCLI-D-11-00015.1.

Rodwell, M. J., and B. J. Hoskins, 2001: Subtropical anticyclones and summer monsoons. *J. Climate*, **14**, 3192–3211, doi:10.1175/1520-0442(2001)014<3192:SAASM>2.0.CO;2.

Romatschke, U., and R. A. Houze, 2013: Characteristics of precipitating convective systems accounting for the summer rainfall of tropical and subtropical South America. *J. Hydrometeor.*, **14**, 25–46, doi:10.1175/JHM-D-12-060.1.

Salio, P., M. Nicolini, and E. J. Zipser, 2007: Mesoscale convective systems over southeastern South America and their relationship with the South American low-level jet. *Mon. Wea. Rev.*, **135**, 1290–1309, doi:10.1175/MWR3305.1.

Saulo, A. C., M. E. Seluchi, and M. Nicolini, 2004: A case study of a Chaco low-level jet event. *Mon. Wea. Rev.*, **132**, 2669–2683, doi:10.1175/MWR2815.1.

Seluchi, M. E., and A. C. Saulo, 2003: The northwestern Argentinean low: A study of two typical events. *Mon. Wea. Rev.*, **131**, 2361–2378, doi:10.1175/1520-0493(2003)131<2361:TNALAS>2.0.CO;2.

Siqueira, J. R., and L. A. T. Machado, 2004: Influence of the frontal systems on the day-to-day convection variability over South America. *J. Climate*, **17**, 1754–1766, doi:10.1175/1520-0442(2004)017<1754:IOTFSO>2.0.CO;2.

——, W. B. Rossow, L. A. T. Machado, and C. Pearl, 2005: Structural characteristics of convective systems over South America related to cold-frontal incursions. *Mon. Wea. Rev.*, **133**, 1045–1064, doi:10.1175/MWR2888.1.

Zhou, J., and K.-M. Lau, 1998: Does a monsoon climate exist over South America? *J. Climate*, **11**, 1020–1040, doi:10.1175/1520-0442(1998)011<1020:DAMCEO>2.0.CO;2.